

Design of a Novel Compliant Differential Shape Memory Alloy Actuator*

Zhao Guo, Haoyong Yu, *Member, IEEE*, and Liang-Boon Wee, *Senior Member, IEEE*

Abstract—This paper presents a novel compliant differential (CD) Shape Memory Alloy (SMA) actuator with improved performance compared to traditional SMA actuators. This actuator is composed of two antagonistic SMA wires and a mechanical joint coupled with a torsion spring. The torsion spring is employed to reduce the total stiffness of SMA actuator and improve the range of motion. The antagonistic wires increase the response time as one wire can be heated up while the other wire is still in the cooling process. Dynamic model of this actuator was established for control design. Experimental results proved that this new actuator can provide larger output range of motion and faster response speed than traditional SMA actuators under the same conditions. Sine wave tracking with 0.05 Hz, 0.08 Hz and 0.1 Hz were performed and our results demonstrated that this compliant actuator has good tracking performance under simple PID control.

I. INTRODUCTION

Shape Memory Alloy (SMA) is an intelligent material that can remember its original shape at low temperature and return to the pre-deformed shape by heating above a threshold temperature. This phenomenon known as the Shape Memory Effect (SME) is the result of a phase transformation between martensite and austenite. SMA wire, especially the Nitinol (Ni-Ti) wire, which has a strain rate of up to 8%, is the most commonly used SMA forms for actuator design.

Compared to conventional (electric, hydraulic, and pneumatic) actuators or other advanced (piezoelectric and EAP) actuators, SMA actuators have the advantages of high power to weight ratio, bio-compatibility, small size, and silence operation, and these advantages make them suitable for a wide range of applications [1], such as robotic surgical systems [2] [3], soft robotics [4], and airfoil profile control [5]. However, SMA actuators also have the disadvantages of low energy efficiency, slow response rate, nonlinearity, hysteresis and low strain rate. Special mechanical design and nonlinear control methods are needed to overcome these limitations.

SMA wire can only achieve unidirectional actuation, thus it is necessary to provide a recovery force via a weight, a spring or another antagonistic SMA wire to achieve bidirectional movement. Typically, there are two classes of SMA actuators [6]. One is the bias spring (BS) SMA actuator

composed of a SMA element and a bias spring. This type of actuator has slow response as the response speed is limited by the cooling process. The other type of actuator design consists of two antagonistic SMA elements, called differential (DI) SMA actuator [7]. This type actuator has faster speed of response than the BS SMA actuator, but it consumes more power and the range of motion is restricted by the antagonistic SMA [8]. SMA actuators with larger working range and quicker response are desirable in many fields [9][10][11]. To achieve these goals, a series of new SMA-based actuators or mechanisms have been developed. For instance, Zhang and Yin [12] presented a SMA-based artificial muscle composed of 16 parallel SMA wires and a simple linear spring to improve the driving force and mimic the character of human muscle. Grant and Hayward [13] developed a differential SMA actuator comprised of 12 SMA wires in a helical arrangement to produce larger movements. Park, *et al* [14] proposed a differential spring-biased SMA actuator for a bio-mimetic artificial finger. In this design, the spring was directly connected to the SMA wire, which may absorb the contraction length of SMA wires and reduce the range of motion of the joint.

In the fields of assistive and rehabilitation robotics, compliant actuators have attracted considerable attention due to their ability of absorbing shocks, interacting with people safely, storing and releasing energy [15]. Many types of compliant actuators, such as Series Elastic Actuator [16], Pneumatic Artificial Muscle [17] have been developed. However, the utilization of advanced materials such as SMA in compliant actuator has not been well investigated.

The motivation of this paper is to develop a new compliant differential (CD) SMA actuator with a simple structure. A torsion spring is employed to achieve better performance over traditional DI SMA and BS SMA actuators. System models include the dynamics and constitution equations are established for control design. A testing setup was designed to compare the properties of this actuator to the two traditional SMA actuators. Furthermore, the position control of this actuator in step response and sinusoidal tracking was investigated.

II. COMPLIANT DIFFERENTIAL SMA ACTUATOR DESIGN

A. Compliant differential SMA actuator

Inspired by the biological structure of human joint actuated by antagonistic skeletal muscles, we propose a new compliant differential SMA actuator to mimic the extension/flexion motion of the biological joint. As shown in Fig. 1(a), this compliant actuator is composed of two antagonistic SMA wires, a torsion spring and two cylindrical couplers. A load is applied on the coupler #1 by threaded connection. Two

*Research Supported by MINDEF/NUS/JPP-11-03.

Zhao Guo is with Singapore Institute for Neurotechnology (SINAPSE), Department of Bioengineering, National University of Singapore, 9 Engineering Drive 1, Singapore 117575, (e-mail: biegz@nus.edu.sg).

Haoyong Yu is with Singapore Institute for Neurotechnology (SINAPSE), Department of Bioengineering, National University of Singapore, 9 Engineering Drive 1, Singapore 117575, (corresponding author, phone: 65-66011590; fax: 65-6872-3069; e-mail: biehyh@nus.edu.sg).

Liang-Boon Wee is with DSO National Laboratories, 20 Science Park Drive, Singapore 118230, (e-mail: wliangbo@dso.org.sg).

antagonistic SMA wires, behaving like artificial muscles, provide the active force for bi-directional motion control of the couplers. The torsion spring, used to mimic the tendon, is packaged inside the couplers. Two legs of the torsion spring (0° deflection, left hand wind) are restricted by the slots in the couplers. The SMA wires are directly connected to the coupler. The active contraction force produced by the SMA wire can be transmitted from one coupler to the other by the torsion spring. The whole structure is simple and easy to implement for different applications.

In this design, we choose a torsion spring. Its stiffness is lower than that of the SMA wire. The spring will provide the recovery force for the agonist SMA wire and reduce the total stiffness of the actuator. An encoder can be assembled on the axis to get the rotational angle.

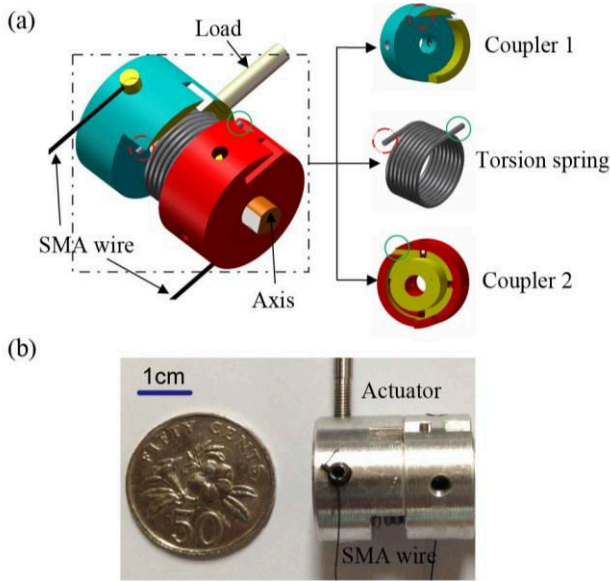


Fig. 1. CAD model and prototype of the compliant differential SMA actuator

B. Three types of SMA actuators

To compare the performance of this actuator with the two traditional SMA actuators, we implement three configurations to represent three types of SMA actuators using the same mechanical setup. They are (a) BS SMA actuator, (b) DI SMA actuator, (c) CD SMA actuator. Figure 2 includes the CAD model and its equivalent mechanical model of each actuator. Two SMA wires generate the tensile force with a variable stiffness k_i and a damping ratio b_i ($i=1, 2$). The torsion spring between two SMA wires transmits the contraction force with a constant stiffness k_s . The damping between the spring and the mechanical part is b_s . m_1, m_2 represents the mass of two parts of the spring coupler respectively. The load applied on the coupler #1 is represented as a mass m_{load} . Because of the small rotational speed, the effect of system damping is neglected. We mainly consider the stiffness of these actuators. The passive stiffness of each actuator is $k_{BS} = k_s$, $k_{DI} = k_2$, $k_{CD} = (k_2 \cdot k_s) / (k_2 + k_s)$

respectively. Due to $k_s < k_2$, the order of the passive stiffness follows $k_{CD} < k_{BS} < k_{DI}$.

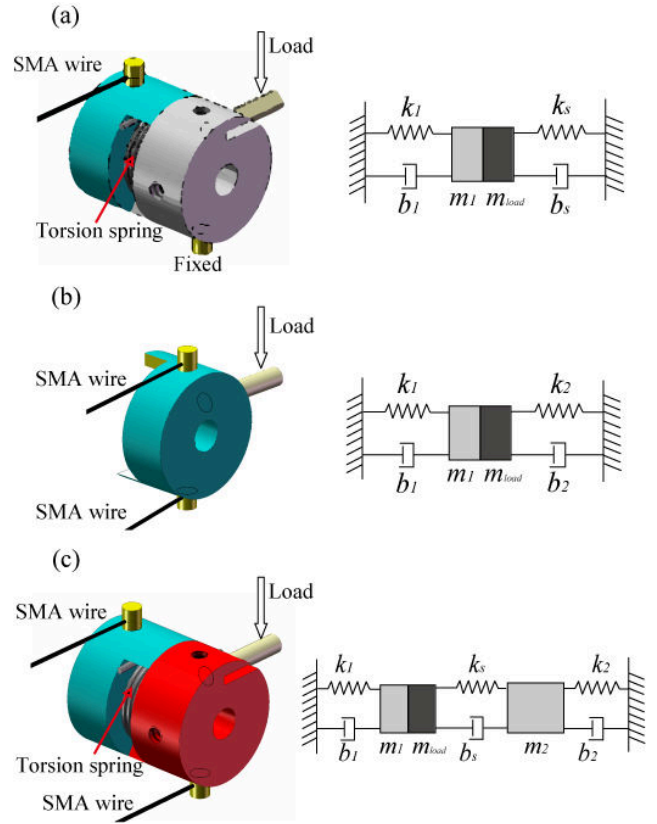


Fig. 2. CAD models and equivalent mechanical models for three SMA actuators: (a) BS SMA actuator; (b) DI SMA actuator; (c) CD SMA actuator.

III. MODELING THE COMPLIANT DIFFERENTIAL SMA ACTUATOR

The model of the actuation system includes the dynamics and kinematics of the actuator as well as the constitutive equations, transformation equations and the heat transfer dynamics of the SMA wire.

A. Dynamics and Kinematics

A simplified model of the actuator is shown in Fig. 3. The couplers are actuated independently under the function of SMA wires, the rotational angle of each coupler is defined as θ_1, θ_2 , which is relative to the y axis.

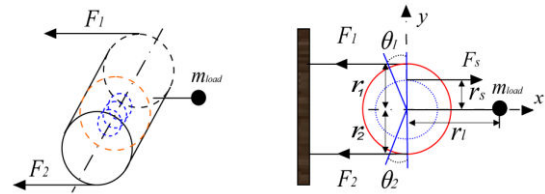


Fig. 3. Schematic diagram of the CD SMA actuator, F_1, F_2 are the active forces of the upper and lower SMA wires respectively, F_3 is the torsion spring force, r_1, r_2 represent the moment arm, r_s is the radius of torsion spring.

The dynamic equation of each coupler is given by

$$\begin{cases} J_T \ddot{\theta}_1 = \tau_1 - \tau_s \\ J_2 \ddot{\theta}_2 = \tau_2 - \tau_s \end{cases} \quad (1)$$

where $J_T = (J_1 + J_m)$, J_i is the inertia of each coupler and the inertia of the load on the actuator's axis is $J_{load} = m_{load} r_i^2$, τ_i is the torque applied by SMA wire. τ_s is the torque from torsion spring. The dynamic model is written as

$$\begin{cases} J_T \ddot{\theta}_1 = F_1 r_1 - k_s (\theta_1 + \theta_2) \\ J_2 \ddot{\theta}_2 = F_2 r_2 - k_s (\theta_1 + \theta_2) \end{cases} \quad (2)$$

The contraction force of the SMA wires

$$F_i = A_i \sigma_i, \quad i=1,2 \quad (3)$$

where A_i is the cross-sectional area, σ_i is the normal stress, which is described by the constitutive model of SMA wire. The strain rate $\dot{\epsilon}_i$ is derived from kinematics as a function of the joint velocity $\dot{\theta}_i$.

$$\dot{\epsilon}_i = -r_i \dot{\theta}_i / l_i, \quad i=1,2 \quad (4)$$

where l_i is the initial length of the SMA wire.

B. Constitutive model

The constitutive model of the SMA wire can be described as the relation of stress σ , strain ϵ and temperature T [18]. Stress is the function of temperature, martensite fraction ξ , and strain. This model can be describe as

$$\dot{\sigma} = E \dot{\epsilon} + \Theta \dot{T} + \Omega \dot{\xi} \quad (5)$$

where E , Θ and Ω are the Young's modulus, thermal expansion factor and phase transformation constant respectively. E is assumed to change linearly between martensite and austenite value E_M and E_A .

C. Phase transformation model

SMA phase transformation takes place between martensite and austenite by heating or cooling. The martensite fraction is a parameter given by $0 \leq \xi \leq 1$. When $\xi = 1$, it means the SMA is completely in the martensite phase. ξ is modeled as a function of SMA temperature and stress [18].

During heating transformation, ξ is given by

$$\text{If } A_s + \frac{\sigma}{C_A} \leq T \leq A_f + \frac{\sigma}{C_A} \\ \xi = \frac{\xi_M}{2} \{ \cos[a_A(T - A_s) + b_A \sigma] + 1 \} \quad (6)$$

During cooling transformation, ξ is given by

$$\text{If } M_s + \frac{\sigma}{C_M} \leq T \leq M_f + \frac{\sigma}{C_M} \\ \xi = \frac{1 - \xi_A}{2} \cos[a_M(T - M_f) + b_M \sigma] + \frac{1 + \xi_A}{2} \quad (7)$$

where a_A , a_M , b_A and b_M are material properties derived from the four transition temperatures, M_f (martensitic finish), M_s (martensitic start), A_s (austenitic start), A_f (austenitic finish), C_A , C_M are material constants, and ξ_M , ξ_A are the initial martensite fractions for each transformation process.

D. Heat transfer model

The SMA heat transfer model describes the rate of temperature due to changes in current in the wire. Part of the power generated by the current actually increases the wire's temperature, while the remaining part is lost. This model can be defined by [19].

$$m_w c_p \dot{T} = \frac{V^2}{R} - h A_w (T - T_{amb}) \quad (8)$$

where m_w is the mass per unit length; c_p is the specific heat; V is the applied voltage; R is the resistance per unit length; h is the heat convection coefficient; A_w is the wire surface area and T_{amb} is the ambient temperature.

Figure 4 shows the block diagram and symbolic representation of the equations involved in the overall mathematical model of the actuator, where θ is the real angular position, θ_r is the desired angular position.

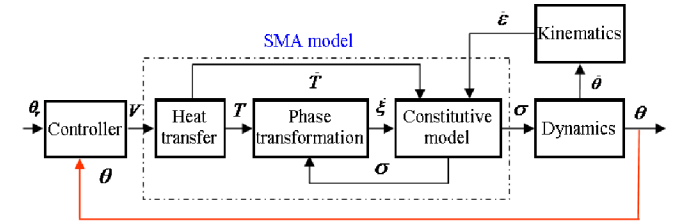


Fig.4. Block diagram of the actuator

E. Controller design

We designed a proportional integral (PI) controller for the position control of SMA actuator by adjusting the voltage on wires. The control structure is shown in Fig. 5. The controller output voltage is expressed as

$$V_{out} = K_p \Delta\theta + K_I \int \Delta\theta dt \quad (9)$$

where $\Delta\theta = \theta_r - \theta$, K_p , K_I are the proportional and integral gains, respectively. V_{out} is restricted in the range of 0~3V to prevent overheating the SMA wires.

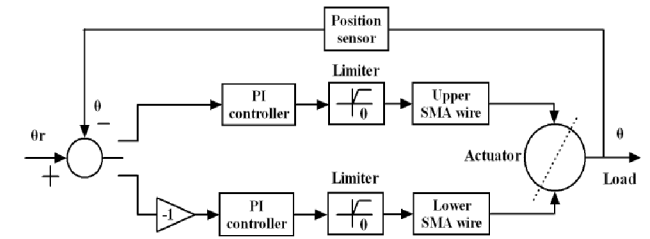


Fig.5. Two channels position controller

The control strategy for each SMA wire is determined based the tracking error $\Delta\theta$. If we set the desired angle in positive value, when $\Delta\theta \geq 0$, the upper wire will be heated and the current on lower wire is zero. When $\Delta\theta < 0$, it means the actual result is overshoot, the lower wire will be heated to reduce the overshoot and the upper wire is in the cooling phase, until the real value is close to the reference.

On the other hand, if we set the desired angle as negative, when $\Delta\theta \leq 0$, the lower wire will be heated and the upper wire is in cooling. When $\Delta\theta > 0$, it also means the result is overshoot, then the upper wire will be heated and the lower wire is in cooling. In this control strategy we can produce a

fast control on the joint motion. The rule for each wire is shown in Equation (10) (11).

$$\text{Upper SMA wire: } \begin{cases} V = V_{out} & \Delta\theta \geq 0 & \text{heating} \\ V = 0 & \Delta\theta < 0 & \text{cooling} \end{cases} \quad (10)$$

$$\text{Lower SMA wire: } \begin{cases} V = V_{out} & \Delta\theta \leq 0 & \text{heating} \\ V = 0 & \Delta\theta > 0 & \text{cooling} \end{cases} \quad (11)$$

IV. EXPERIMENTAL SETUP AND RESULTS

A. Experimental setup

An experimental setup has been developed to evaluate the performance of this CD SMA actuator. A small iron stick is connected to the actuator as the load for testing. Figure 6 shows the schematic diagram of the control hardware and picture of the experimental setup, respectively. Two antagonistic NiTi SMA wires (Dynalloy, Inc.) are selected in our actuator design. Their properties are summarized in Table I. The diameter of each SMA wire d is $250\mu\text{m}$. Angular position is measured by a shaft encoder (Omron E6B2-CWZ1X) with a resolution of 2500 pulses per turn. A NI-PCI-6221 DAQ card is used to collect the data and provide the analog voltage outputs with a full-scale range of ± 10 V to an amplifier. Two channel analog voltages were augmented by the amplifier with a gain of 3.125V/V and applied on two SMA wires separately. The test was implemented on a Lab VIEW platform (National Instruments, Inc.) on a PC.

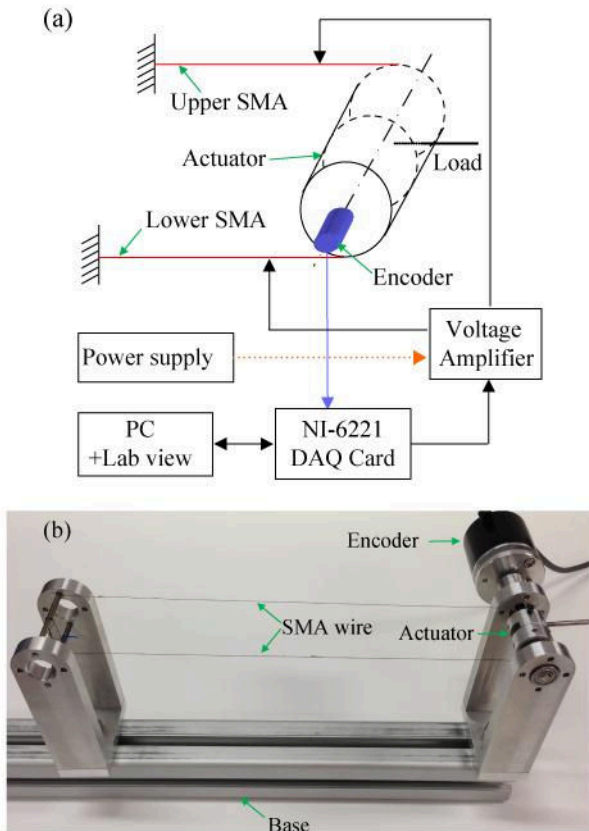


Fig.6. (a) Block diagram configuration of the position control system and (b) experimental setup for testing.

TABLE I. PARAMETERS OF THE CD SMA ACTUATOR

Parameter	Value	Parameter	Value
E_M	28GPa	d	250 μm
E_A	75GPa	A_w	$290.45 \times 10^{-6} \text{m}^2$
ρ	6.45g/cm ³	T_{umb}	20°C
A_s	88°C	C_A	10MPa/°K
A_f	98°C	C_m	10MPa/°K
M_s	72°C	C_p	320J/kg°C
M_f	62°C	m_w	$6.8 \times 10^{-4} \text{kg/m}$
R	20 Ω/m	r_1, r_2	10mm
l_1, l_2	0.37 m	σ_0	25MPa
k_s	0.0018N·m/1°	k_1, k_2	3714–10348N/m
m_1, m_2	10g	r_2	7.5mm

B. Performance comparison for three SMA actuators

We compare this new SMA actuator with the other two SMA actuators in two aspects: range of motion and response speed. We apply the same output voltage (1V) on the upper SMA wire of these actuators. The current across the SMA wire is 0.42A, and the lower SMA wire works as a variable stiffness spring. According to the Young's modulus of SMA wire in two transformation phases, the range of its stiffness is linearly changed from $3714\text{N}\cdot\text{m}$ to $10384\text{N}\cdot\text{m}$. The stiffness of torsion spring is selected as $0.0018\text{N}\cdot\text{m}/1^\circ$; its equivalent stiffness to extension spring is $1031\text{N}\cdot\text{m}$. The stiffness of torsion spring is lower than that of the SMA wire. Experimental results for three actuators, including the heating and cooling phases of the upper SMA wire, are shown in Fig. 7. The results indicate that the CD SMA actuator provides largest angular range of motion. The maximum angular motion of the CD SMA actuator is close to 30° , while BS SMA actuator is limited to 20° and DI SMA actuator provides only 13° . This limitation in angular motion is due mainly to the high stiffness of the antagonist SMA wire.

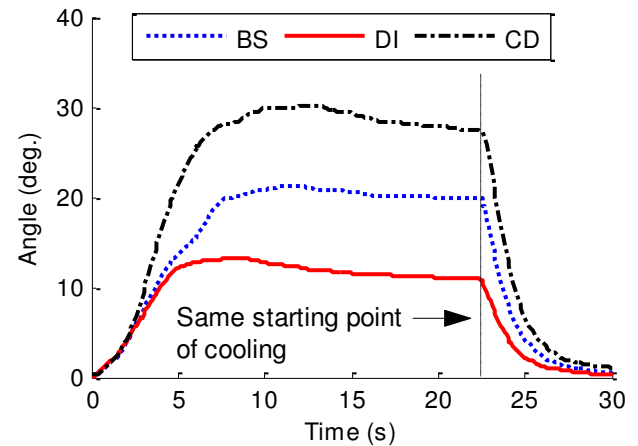


Fig.7. Experimental angular position of three SMA actuators under the same applied current.

The dynamic response of the three actuators show a slight position overshoot before reaching steady-state, see Fig.7. This behavior is explained with the aid of the heat dynamics, equation (8). During the heating phase, the SMA wire

undergoes a phase change that persists till an energy balance between the power input and the power loss is reached. This energy transfer also corresponds to the temperature response of SMA wire. During the cooling phase, we observed that the rate at which the CD SMA actuator returned to the relaxed state is faster than the other actuators. This faster rate of the CD SMA actuator is provided by stored energy in the torsion spring. The above results clearly indicate that the CD SMA actuator provide large working range under the same current stimulating condition, as well as more efficient energy utilization compared to the other two actuators.

C. Step response

The experimental responses to a series of step inputs were examined on this new SMA actuator. A single channel and two-channel controls were applied for a cooling speed performance comparison. In one channel control, the upper SMA wire was actively heated and the antagonistic SMA wire was passive. In two-channel control, when the real position was larger than the reference, the antagonistic SMA wire would be activated to reduce the overshoot and increase the cooling process.

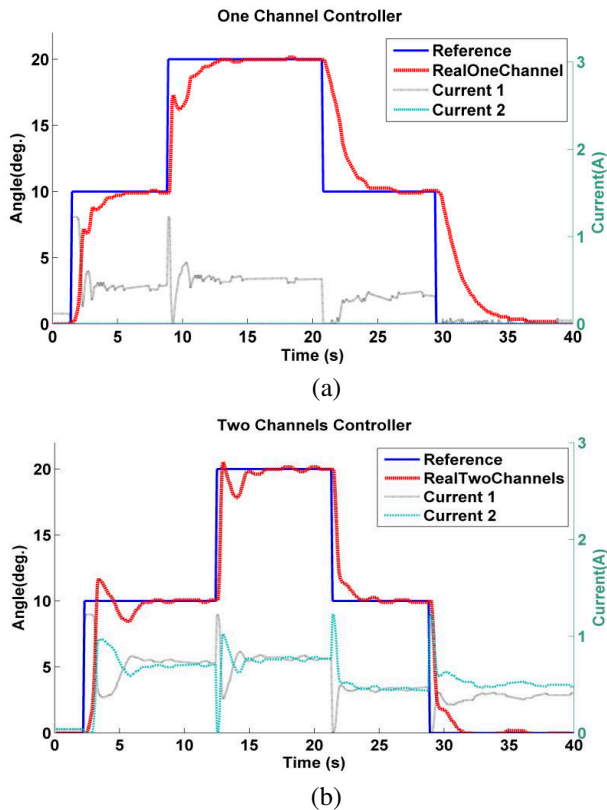


Fig.8. (a) One channel control for the CD SMA actuator and (b) two channels control for the CD SMA actuator

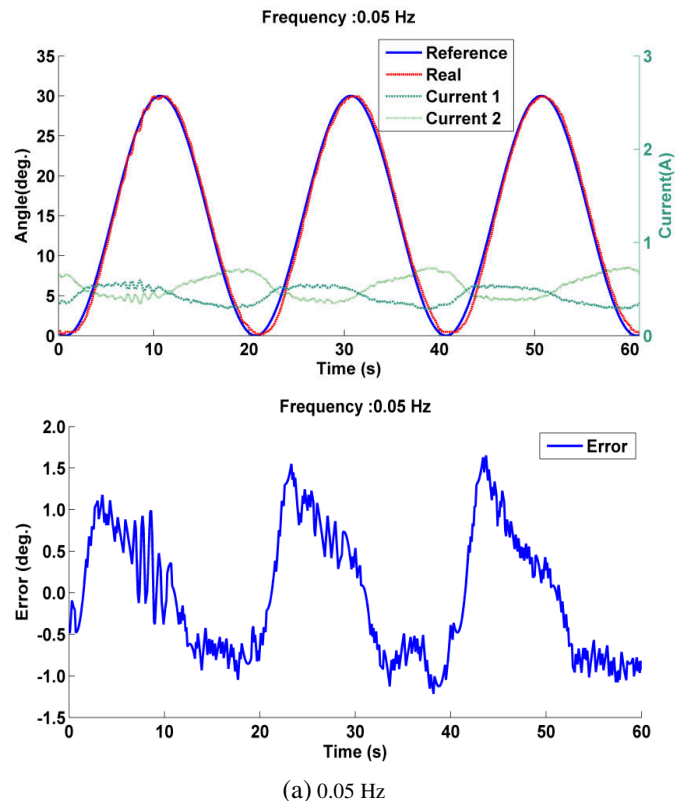
Figure 8(a) shows responses to desired steps of 10° and 20° in one channel control. In terms of time-domain specification, during the heating phase, the average rise time to the 10° step input is approximately 3.5 s. For the response to a 20° , it is slightly long and requires approximately 5 seconds. This is expected, as the set point is further away from the zero position, so it takes a longer time for the actuator to reach the desired set point. During the cooling

phase, the average fall time from 20° to the 10° and from 10° to 0° is approximately 6 seconds. The joint angle reduced slowly to the set point under the recovery force from the torsion spring.

To reduce the fall time, a second PI controller was provided to the lower SMA wire. Figure 8(b) shows the step responses to the desired steps of 10° and 20° . Compared to the one channel control, the rise time reduces to about 1s. Despite an overshoot in the heating phase, the position angle tends to stable soon due to the integral gain. Meanwhile during the cooling phase of upper SMA wire, the second SMA wire would be heated to increase the cooling speed. The fall time of step input from 20° to 10° , 10° to 0° reduces to about 2.5 s. These figures clearly show that the rise and fall times of step responses have decreased significantly. The response speeds both in the heating and cooling phase are increased. This clearly demonstrates that our proposed actuator design and control method have achieved better performance than the conventional SMA actuator.

D. Tracking response

This part presents the tracking responses of the CD actuator to a series of sinusoidal inputs with frequencies of 0.05 Hz, 0.08Hz and 0.1 Hz using the proposed control method. It can be seen that the tracking performance for 0.05 Hz is better than 0.08Hz and 0.1Hz in Fig. 9 (a) (b) (c). The tracking error for 0.05Hz, 0.08Hz and 0.1 Hz is about $-1^\circ \sim 1^\circ$, $-1^\circ \sim 1.5^\circ$, $-2.5^\circ \sim 1.5^\circ$ respectively. As the frequency of the sine wave increases, the error increases gradually, the system begins to lag behind the desired response due to the slow response speed of the actuator.



(a) 0.05 Hz

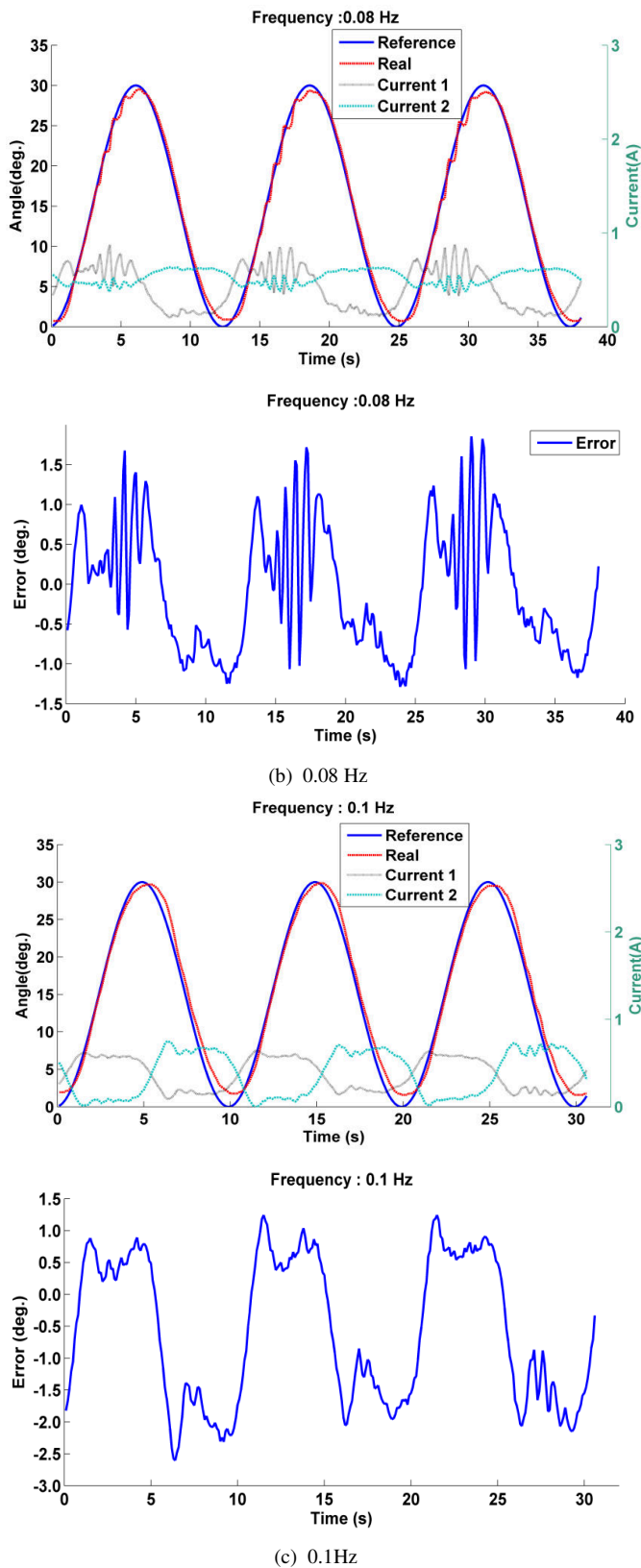


Fig.9. Sine tracking response with (a) 0.05 Hz, (b) 0.08 Hz and (c) 0.1Hz.

V. CONCLUSION

A novel CD SMA actuator using two antagonistic SMA wires and a torsion spring has been proposed to improve the performance of traditional SMA actuators. Experiments for

this new actuator and the two conventional SMA actuators have been conducted for performance comparison. Position control experiments for step response and sine wave tracking demonstrated that this novel compliant actuator has faster response speed, larger output range. The response speed of SMA actuator can be further increased to faster and more robust joint motion with better control methods. We are currently developing advanced controller to improve the performance of this actuator and developing applications for rehabilitation robotic and surgical robotic systems.

REFERENCES

- [1] A. Nespole, S. Besseghini, S. Pittaccio, E. Villa, and S. Viscuso, "The high potential of shape memory alloys in developing miniature mechanical devices: A review on shape memory alloy mini-actuators," *Sensors and Actuators A*, vol. 158, pp. 149-160, Mar 2010.
- [2] P. Sears and P. Dupont, "A steerable needle technology using curved concentric tubes," in *IEEE/RSJ Int. Conf. Intell. Robots Syst.*, Beijing, China, from Oct. 9-15, 2006, pp. 2850-2856.
- [3] R. Webster, A. M. Okamura, and N. J. Cowan, "Toward active cannulas: Miniature snake-like surgical robots," in *IEEE/RSJ Int. Conf. Intell. Robots Syst.*, Beijing, China, from Oct. 9-15, 2006, pp. 2857-2863.
- [4] S. Kim, E. Hawkes, K. Choy, M. Joldaz, J. Foley, and R. Wood, "Micro artificial muscle fiber using NiTi spring for soft robotics," in *IEEE/RSJ Int. Conf. Intell. Robots Syst.*, St. Louis, USA, from Oct. 11-15, 2009, pp. 2228-2234.
- [5] F. Peng, X.-X. Jiang, Y.-R. Hu, and A. Ng, "Application of shape memory alloy actuators in active shape control of inflatable space structures," in *Proc. IEEE Conf. Aerosp.*, 2005, pp. 1-10.
- [6] C. Liang and C. Rogers, "Design of shape memory alloy actuators," *J. Intell. Mater. Syst. Struct.*, vol. 8, pp. 303-313, 1997.
- [7] R. B. Gorbet and R. A. Russell, "A novel differential shape memory alloy actuator for position control," *Robotica*, vol. 13, pp. 423-30, 1995.
- [8] M. Moallem and V. Tabrizi, "Tracking control of an antagonistic shape memory alloy actuator pair," *IEEE Trans. Control Syst. Technol.*, vol. 17, pp. 184-190, 2009.
- [9] H. Ashrafioun, M. Eshraghi, and M. H. Elahinia, "Position control of a three-link shape memory alloy actuated robot," *J. Intell. Mater. Syst. Struct.*, vol. 17, pp. 381-392, 2006.
- [10] S. Z. Yan, X. J. Liu, F. Xu, and J. H. Wang, "A gripper actuated by a pair of differential SMA springs," *J. Intell. Mater. Syst. Struct.*, vol. 18, pp. 459-466, May 2007.
- [11] E. T. Esfahani and M. H. Elahinia, "Stable walking pattern for an SMA-actuated biped," *IEEE-ASME Trans. Mechatron.*, vol. 12, pp. 534-541, Oct 2007.
- [12] J. J. Zhang and Y. H. Yin, "SMA-based bionic integration design of self-sensor-actuator-structure for artificial skeletal muscle," *Sensors and Actuators A*, vol. 181, pp. 94-102, Jul 2012.
- [13] D. Grant and V. Hayward, "Variable structure control of shape memory alloy actuators," *IEEE Control Syst. Mag.* vol. 17, pp. 80-88, Jun 1997.
- [14] V. Bundhoo, E. Haslam, B. Birch, and E. J. Park, "A shape memory alloy-based tendon-driven actuation system for biomimetic artificial fingers, part I: design and evaluation," *Robotica*, vol. 27, pp. 131-146, 2009.
- [15] R. Van Ham, T. G. Sugar, B. Vanderborcht, K. W. Hollander, and D. Lefeber, "Compliant Actuator Designs," *IEEE Robot. Autom. Mag.*, vol. 16, pp. 81-94, Sep 2009.
- [16] G. A. Pratt and M. M. Williamson, "Series elastic actuators," in *IEEE/RSJ Int. Conf. Intell. Robots Syst.*, Pittsburgh, USA, from Aug. 5-9, 1995, pp. 399-406.
- [17] C. P. Chou and B. Hannaford, "Measurement and modeling of McKibben pneumatic artificial muscles," *IEEE Robot. Autom. Mag.*, vol. 12, pp. 90-102, Feb 1996.
- [18] C. Liang and C. Rogers, "One-dimensional thermomechanical constitutive relations for shape memory materials," *J. Intell. Mater. Syst. Struct.*, vol. 1, pp. 207-234, 1990.
- [19] A. R. Shahin, P. H. Meckl, J. D. Jones, and M. A. Thrasher, "Enhanced Cooling of Shape-Memory Alloy Wires Using Semiconductor Heat-Pump Modules," *J. Intell. Mater. Syst. Struct.*, vol. 5, pp. 95-104, Jan 1994.